CrystEngComm

Accepted Manuscript

ROYAL SOCIETY OF CHEMISTRY

www.rsc.org/crystengcomm

Graphical abstract

Pd-Pt alloy nanohypercubes were fabricated by reducing Pd and Pt precursors simultaneously with tetraethylene glycol in one step process under microwave irradiation for only 100 sec. Iodide ions were critical to their syntheses.

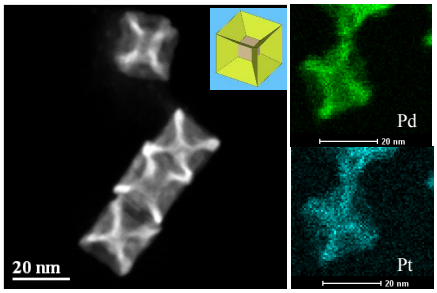

TOC Text:
Pd-Pt alloy nanohypercubes

Cite this: DOI: 10.1039/c0xx00000x

www.rsc.org/xxxxxx

COMMUNICATION

Controlled Synthesis of Pd-Pt Alloy Nanohypercubes under Microwave Irradiation†

Lei Dai,[a] Yanxi Zhao,[a] Quan Chi,[a] Tao Huang,*[a] Hanfan Liu*[a,b]

Received (in XXX, XXX) Xth XXXXXXXXX 20XX, Accepted Xth XXXXXXXXX 20XX

DOI: 10.1039/b000000x

Pd-Pt alloy hypercubic nanostructures were successfully fabricated by reducing Pd and Pt precursors simultaneously in one step process under microwave irradiation for only 100 sec without using any sacrificial templates. Together with the use of tetraethylene glycol (TEG) as both a solvent and a reducing agent, the presence of KI was critical to the formation of Pd-Pt alloy nanohypercubes. The as-prepared Pd-Pt alloy nanohypercubes improved the electrocatalytic activities.

Noble metal nanostructures with concave surfaces or hollow cores have emerged as an important class of nanomaterials and attracted considerable attention for decades owing to their unique catalytic, electronic, optical, magnetic and biomedical applications.[1] The physical and chemical properties of these metal nanocrystals are strongly dependent upon their sizes, shapes, compositions, crystallinities and structures. So, a lot of efforts have been devoted to the syntheses of special nanostructures with well-defined shapes. To date, most of the obtained polyhedra with concave surfaces or hollow structures were made of a single metal such as concave cubes,[2] concave tetrahedra,[3] cages[1e,4] and naoframes,[5] though a few similar bimetallic nanocrystals with core-shell or alloy structures such as Pd@Cu core-shell nanocubes,[6] Pd-Rh core-frame nanocubes,[5a] concave[7] or hollow Pd-Pt alloy nanocubes,[8] nanocages,[9] Pt-Au alloy nanocubes,[10] AuAg double-walled nanoboxes,[9a] octahedral Au-Ag nanoframes,[11] octapodal Au-Pd nanoparticles[12], and Au-Pd core-shell heterostructures[13] were also obtained. Generally, however, bimetallic nanocrystals with concave surfaces were tuned up by overgrowth or etching routes, while hollow nanostructures were mainly generated by galvanic replacement reactions or/and Kirkendall effect.[14] In addition, sacrificial templates as well as necessary post-treatment were usually used in fabricating these kinds of nanostructures, especially hollow bimetallic nanocrystals.[14] Therefore, to develop a facile and simple method for synthesis of bimetallic nanoparticles with specific morphologies remains a great challenge.

Microwave dielectric heating has been extensively applied to the synthesis of metal nanoparticles due to its advantages compared with conventional heating, such as fast, uniform and deep heating, low cost, and high energy efficient, etc.[15] Herein, microwave irradiation was employed in the shape-controlled synthesis of bimetallic alloy nanocrystals and a unique single-crystalline Pd-Pt alloy hypercubic nanostructure, a four-dimensional analogue, with both special concave surfaces and a hollow interior was synthesized by one-pot strategy under microwave irradiation in an extremely short time without using any sacrificial template and any post-treatment. The use of iodide ions was critical to the formation of the Pd-Pt hypercubic nanostructures. The electrocatalytic propeties of the as-prepared Pd-Pt alloy nanohypercubes were also investigated.

In a typical synthesis, together with the use of tetraethylene glycol (TEG) as both a solvent and a reducing agent, a mixed solution of sodium tetrachloropalladate (II) (Na_2PdCl_4) and hexachloroplatinic acid (H_2PtCl_6) in TEG was heated for 100 sec in the presence of polyvinylpyrrolidone (PVP) and potassium iodide (KI) under microwave irradiation. The resulting products were collected by centrifugation and treated several times with ethanol. The representative TEM images of the as-prepared Pd-Pt nanocrystals are shown in **Fig. 1**a and b, as well as **Fig. S1, ESI†**, which were obviously different from the previously reported Pd-Pt bimetallic concave nanocubes.[7] As can be seen, most of the projections of the resulting nanoparticles under TEM illustrated as Schlegel diagrams (**Fig. S2, ESI†**), as shown in the inset of **Fig. 1**b, which reflects the relationship between vertices in one hypercube and commonly used as a means of visualizing 4-dimensional polytopes, revealing that the resulting nanostructures were present as hypercubes. The average size was about 22 ±1.2 nm in edge length. The hypercubic feature of the obtained nanostructures was further confirmed by high-angle annular dark-field scanning transmission electron microscopy (HAADF-STEM) analysis (**Fig. 1**c, and **Fig. S3, ESI†**), which was agreement with the geometric model as the inset shown in **Fig. 1**c.

Furthermore, to verify the hypercubic nanostructure, an etching was conducted in an aqueous solution of the as-prepared Pd-Pt nanohypercubes by using $FeCl_3$ which is a well-known wet etchant for precious metals.[5a,16] Interestingly, all the lateral walls and outside edges disappeared after etching, which may be ascribed to their ultrathin feature, and highly branched structures with one hollow interior and eight branches along the linkages between vertices in each one were left behind, as shown in **Fig. 1**d. Due to a higher reduction potential of Fe(III)/Fe(II) pair (+0.771 V *vs.* RHE) than that of $PdCl_4^{2-}$/Pd pair (+0.59 V *vs.* RHE),[5a] Pd atoms in the lateral walls were selectively removed through oxidative etching, resulting in the collapse of the ultrathin lateral walls. This result confirmed the hypercubic

feature of the as-prepared Pd-Pt nanostructures.

The structural model is shown in **Fig. 2S**, **ESI†**. It consists of 12 lateral walls (24 side faces) and a cubic core. Notably, the as-obtained hypercubic nanostructures demonstrate inner joins between vertices, while the side faces are ultrathin. These features are obviously different from those reported concave nanocubes or highly concave nanoframes.[2h,5b] Moreover, the little cubic cores of the as-obtained Pd-Pt nanohypercubes were present in hollow feature, which can be well visualized from TEM (**Fig. 1**b, d and **Fig. S1, ESI†**), HAADF-STEM images (**Fig. 1**c and **Fig. S3, ESI†**).

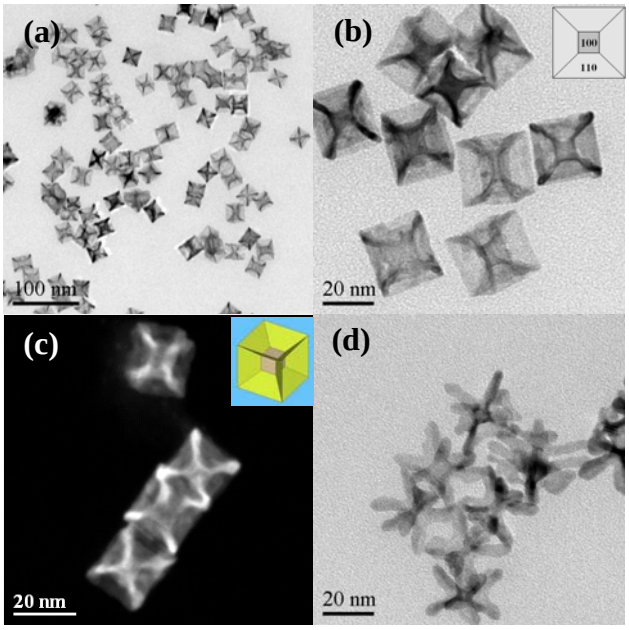

Fig. 1 (a) and (b) TEM images with different magnifications. The inset of (b) is a Schlegel diagram; (c) HAADT-STEM images of the as-prepared Pd-Pt hypercubes; (d) TEM images after etching the lateral walls of Pd-Pt hypercubes. The inset of (c) is the corresponding structure model.

Fig. 2a and b show the HRTEM images of individual Pd-Pt alloy nanohypercube along [100] zone axis and the corresponding fast Fourier transform (FFT) pattern (the inset of **Fig. 2**b). **Fig. 2**c and d show the HRTEM images along [110] zone axis and the corresponding FFT pattern (the inset of **Fig. 2**d). The HRTEM measurement showed the lattice fringes with an interplanar spacing of 2.3, 2.0 and 1.4 Å can be indexed to {111}, {200} and {220} planes of Pd-Pt nanohypercube. As confirmed by HRTEM images and the corresponding FFT patterns, well-resolved and continuous crystal lattice clearly revealed a single crystalline structure and good crystallinity for an individual hypercubic Pd-Pt nanocrystal. The single-crystal feature was ascribed to their same face-centered cubic (*fcc*) structure and negligible lattice mismatch between Pt and Pd. As a result, each nanohypercube was consisted of twenty-four (110) isosceles-trapezium lateral walls and six square (100) faces (the cubic core).

In addition, XRD pattern shows five characteristic peaks at 40.2°, 46.8°, 68.2°, 82.1° and 86.7°, corresponding to the (111), (200), (220), (311) and (222) lattice planes (**Fig. S4, ESI†**), which were consistent with the standard diffraction pattern for *fcc* Pd and Pt. From the well-known Scherrer equation,[17] the mean particle size was calculated to be 23.4 nm, which was consistent with the observation by TEM on the whole.

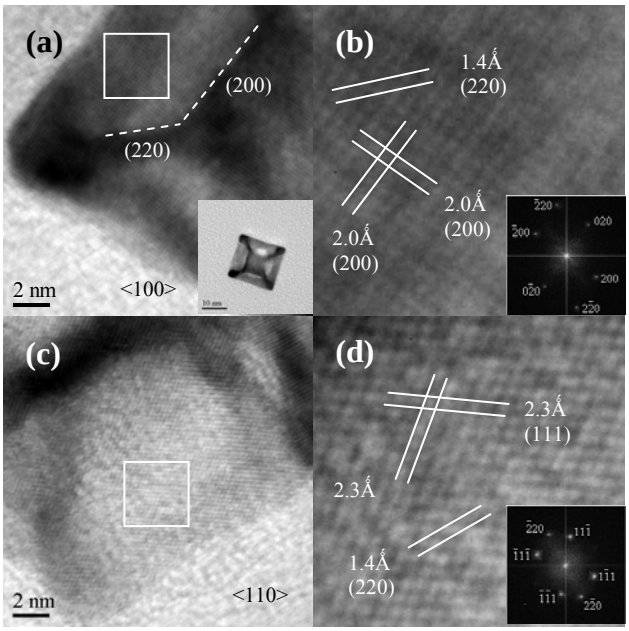

Fig. 2 (a) HRTEM image of a part of individual nanohypercube projected along [100] zone axis; (b) the corresponding enlarged HRTEM of the selected area in (a); (c) HRTEM image of a part of individual nanohypercube projected along [110] zone axis; (d) the corresponding enlarged HRTEM of the selected area in (c). The insets of (b) and (d) are the corresponding FFT pattern, respectively.

XPS measurement showed the binding energy of $Pd3d_{5/2}$ and $Pd3d_{3/2}$ at 334.56 and 339.89 eV, while $Pt4f_{7/2}$ and $Pt4f_{5/2}$ at 70.38 and 73.78 eV, respectively (**Fig. S5, ESI†**). The binding energies were coincident with the standard values (335.10 and 340.36 eV for $Pd3d_{5/2}$ and $Pd3d_{3/2}$, 70.80 and 74.15 eV for $Pt4f_{7/2}$ and $Pt4f_{5/2}$),[18] indicating Pt(0) and Pd(0) with zero oxidation states.

The elemental composition of the Pd-Pt nanohypercube was analyzed by energy dispersive X-ray spectroscopy (EDX). The EDX mapping clearly showed that the as-prepared hypercubic nanostructure was made of a Pd-Pt alloy, as shown in **Fig. 3**a (HAADT-STEM image), b (green, Pd) and c (cyan, Pt). The hollow feature of the inner cubic core was also identified from the EDX mapping. Interestingly, obvious differences for the relative contents of Pd and Pt were observed in different regions of a Pd-Pt nanohypercube. EDX spot analyses for different selected regions (spot 1, 2, and 3 in **Fig. 3**d) were conducted and exhibited the presence of 72% Pd and 28% Pt at the linking part between the vertices (spot 1), 40% Pd and 60% Pt in the lateral wall (spot 2), 65% Pd and 35% Pt at the hollow cubic interior (spot 3), respectively. The Pd/Pt atomic ratios at the spot 1, 2 and 3 are plotted in **Fig. 3**e, corresponding to the EDX spectra (**Fig. S6, ESI†**) on spot analyses. The distribution differences among the different regions in a Pd-Pt alloy hypercube confirmed that its formation involved several different processes. The Pd-Pt alloy was also supported by EDX line-scan profile along the frontage diagonal of a single particle (**Fig. 3**f).

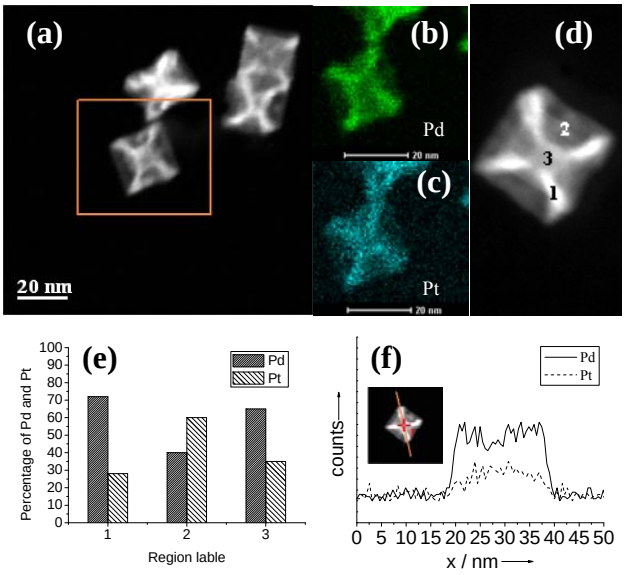

Fig. 3 (a) HAADT-STEM image for EDX mapping; (b) and (c) EDX mapping of the selected individual Pd-Pt hypercube in (a), corresponding to the distribution of Pd (green) and Pt (cyan), respectively. (d) HAADT-STEM image of a single Pd-Pt hypercube with three selected areas for EDX spot analysis. (e) The percentage of Pd and Pt atoms corresponding to region 1, 2, 3 in (d), respectively, obtained by EDX analysis. (f) Line-scanning profile along the frontage diagonal.

To better understand the forming process of the Pd-Pt nanohypercubes in one step under microwave irradiation, the dependence of the morphological feature of the Pd-Pt nanocrystals upon the reaction time was investigated. When the irradiation time was 80 s, nanocubes with smaller size and inconspicuous concavities were produced and no void space in the centre can be distinguished (**Fig. 4**a), while the reaction time was increased to 120 or 140 s, the mean size of the as-obtained hypercubes with poor dispersion increased and the outside frames became thicker due to overgrowth (**Fig. 4**b and c).

Furthermore, it was found that the use of appropriate amount of KI was critical to the formation of Pd-Pt alloy hypercubes. In the absence of KI, only irregular small nanoparticles were produced (**Fig. 4**d). With adding a little amount of KI, hypercubic feature was obscure (**Fig. 4**e). In contrast, Pd-Pt alloy hypercubes with porous side faces and thicker outside frames were generated with using too much amount of KI (**Fig. 4**f). Under the same conditions, an equal amount of KCl or KBr was used instead of KI, no hypercubic structure was obtained (**Fig. S7, ESI†**). These results confirmed that the formation of the Pd-Pt alloy nanohypercubes should be attributed to the existence of I^- ions. To manipulate the reducing kinetics would be favorable for the growth of Pd-Pt alloy hypercubes. On the one hand, the addition of KI reduced the potential of Pd(II) and Pt(IV) ions due to the formation of a more stable coordinated anion $[PdI_4]^{2-}$ and $[PtI_6]^{2-}$, so that their reducing rates became slow. Moreover, the reduction potential of Pt(IV) species (-0.09 V *vs*. SCE) was more negative than that of Pd(II) species(+0.28 V *vs*. SCE) due to the coordination of I^- ions (**Fig. S8, ESI†**), so that the reduction of Pt(IV) ions would lag behind that of Pd(II) ions. UV-vis absorption measurements confirmed the transformation of the coordinated anions in the presence of I^- ions. After KI was introduced, remarkable changes in absorption spectra were observed for both Na_2PdCl_4 and H_2PtCl_6 in water solution. The absorption bands enhanced and red shifts occurred, accompanying with changes in color of solution (**Fig. S9, ESI†**). The similar changes were also observed in TEG solution except that a special absorption feature was present for KI, which may be attributed to the interaction between KI and TEG (**Fig. S10, ESI†**). On the other hand, microwave irradiation changed the growth kinetics by its specific nonthermal effects because microwave irradiation directly activated most molecules and energy transfer occurred in less than a nanosecond (10^{-9}s),[19] promoting the reaction to occur immediately and finish in a rather short time. In addition, the microwave energy penetrated the crystal nucleus, facilitating preferential crystal growth. However, it was impossible to obtain the Pd-Pt alloy nanohypercubes in absence of KI under the same conditions.

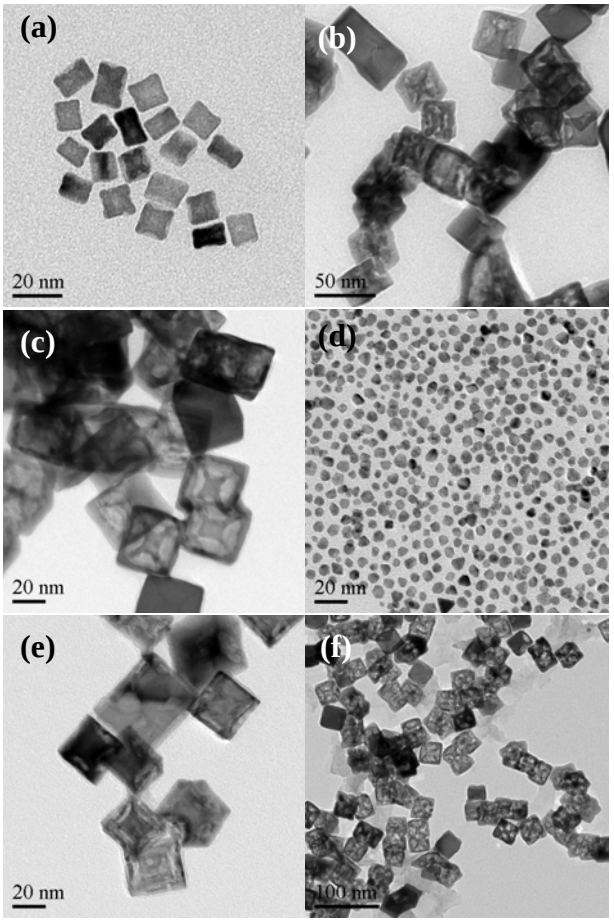

Fig. 4 TEM images of nanoparticles collected from the reactions with different irradiation time or different amount of KI under the same other conditions with the typical experiments. (a) 80 s; (b) 120 s; (c) 140 s; (d) 0 mg of KI; (e) 25 mg of KI; (f) 100 mg of KI.

Therefore, it can be suggested that the formation of Pd-Pt alloy hypercubic nanostructures was dependent on the initial formation of Pd seeds followed by the simultaneous or sequential action of galvanic replacement and the co-deposition. Firstly, we supposed that the selective adsorption of I^- ions on the {100} surface of Pd

nucleus would induce the formation of the primary Pd nanocubes at the initial stage. The effect of halide anions on the anisotropic noble metal nanocrystal growth and the selective adsorption of halide ions on {100} facets of various metals have been demonstrated,[7,8a,20] as evidenced by the formation of Pd nanocubes[8a] or Pd nanowires[20b] enclosed by {100} facets owing to the selective adsorption of I^- ions on Pd {100} facets. Subsequently, Pt(IV) ions were reduced by galvanic replacement reaction and Pt(0) atoms deposited onto the Pd {100} surfaces. Moreover, the strong coordination of I^- ions to Pd(II) ions as well as the microwave irradiation accelerated the galvanic replacement between Pd nanocubic particles and Pt(IV) ions, and hence a fast outward diffusion of Pd atoms to create the hollow inner cores. Meanwhile, the microwave energy penetration is beneficial to alloying. Finally, the selective adsorption of I^- ions prevented the deposition of the newly generated Pd and Pt atoms onto the {100} faces, but the exposed corners and edges, which were composed with (111) and (110) facets respectively, of the nanocubic cores provided opportunities for the deposition of Pd and Pt atoms. As the reaction continued, the Pd(II) and Pt(IV) ions were co-reduced by TEG due to a fast and deep heating under microwave irradiation, the newly formed Pd and Pt atoms were co-deposited preferentially onto the corners and edges of the Pd nanocubes simultaneously along <111> and <110> directions, resulting in a synchronously outward growth of the corners and the edges, and therefore the formation of Pd-Pt alloy nanostructure with hypercubic shapes. The microwave irradiation in this reaction assisted in forming Pd-Pt alloy hypercubes by promoting the reduction, diffusion and co-deposition. Nevertheless, accompanied with the co-deposition process, the galvanic replacement facilitated a faster oxidation and diffusion of Pd atoms followed by reduction of Pt(IV) ions and re-deposition of Pt atoms in the lateral walls along edges than at corners. So, a higher percentage composition of Pt atoms was present at the isosceles-trapezium lateral walls than the linkage part between vertices (**Fig. 3**e, and **Fig. S6, ESI†**). It seemed that ultrathin lateral walls were present within all Pd-Pt alloy hypercubes because of a rapid co-reduction and fast galvanic replacement under microwave irradiation. On the other hand, the strong adsorption of I^- ions on {100} planes was responsible for the generation of the ultrathin lateral walls of the Pd-Pt alloy hypercubes. However, the lateral walls became thicker due to an overgrowth resulted from more diffusion and re-deposition with a more reaction time or small amount of KI (**Fig. 4**c and e). While a more amount of KI was used, the excessive adsorption of I^- ions made the lateral walls more thin, the faster oxidation and diffusion of Pd atoms due to the galvanic replacement reaction between Pd atoms and Pt(IV) ions led to partial ablation of the ultrathin isosceles-trapezium lateral walls, generating porous walls. Meanwhile, the co-reduction of Pd(II) and Pt(IV) ions and preferential re-deposition of Pd and Pt atoms on the external edges led to thicker outside frames (**Fig. 4**f). In addition, the formation of other polyhedra in the case with KBr or KCl may be ascribed to the weaker adsorption of Br^- or Cl^- ions.[20g]

It was noteworthy that well-defined Pd-Pt hypercubes were also generated when $Pd(acac)_2$ was used as the initial Pd precursor instead of Na_2PdCl_4 under the same conditions (**Fig. S11, ESI†**). This further indicated that $[PdI_4]^{2-}$ was the exact precursor in the presence of KI although different palladium salt was introduced initially into the reaction system. Similar results were observed for other palladium salts such as $PdCl_2$, $Pd(Ac)_2$ and $Pd(NO_3)_2$ though the as-prepared hypercubic structures were not ideal and had larger cubic cores (**Fig. S11, ESI†**). These differences may be ascribed to the blocking effects of other anions such as Ac^- or NO_3^- anions upon the adsorption of I^- ions on the Pd (100) facets, resulting in the atomic addition of the newly produced Pd and Pt atoms on the Pd (100) facets.

It was also found that PVP was important but not essential for the formation of Pd-Pt alloy hypercubes. Without or with a little amount of PVP, Pd-Pt hypercubes can be also produced but heavily aggregated (**Fig. S12, ESI†**), indicating that PVP served mainly as a protecting and a dispersing agent for the products.

The dominantly exposed {110} planes were further verified by CO stripping experiments. Only one CO electro-oxidation (CO_{ex}) peak at 0.72 V (versus SCE) was observed in 0.1M $HClO_4$ solution (**Fig. S13, ESI†**), which should be assigned to CO stripping on {110} facets in Pd-Pt alloy hypercubes.[21] It was consistent with the HRTEM observation.

The catalytic activities of the as-prepared Pd-Pt alloy nanohypercubes were investigated by electrocatalytic oxidation of formic acid and methanol. Commercial Pt black was used as a reference for comparison. **Fig. 5a** shows the cyclic voltammetry (CV) curves for the electro-oxidation of formic acid. The peak current densities were measured to be 1.52 and 0.64 $mA \cdot cm^{-2}$ on Pd-Pt alloy hypercubes and Pt black at 0.71 and 0.65 V in 0.5M H_2SO_4, respectively. The electrocatalytic activity of Pd-Pt nanohypercubes was about 2.4 times greater than that of Pt black for the electro-oxidation of formic acid. Similar behaviors were also found in the electro-oxidation of methanol. The current density was 1.0 $mA \cdot cm^{-2}$ on Pd-Pt alloy hypercubes at 0.61 V in 0.1M $HClO_4$, presenting about 2.3 times greater than that of Pt black on which it was 0.44 $mA \cdot cm^{-2}$ at 0.68 V, as shown in **Fig. 5b**. These results revealed that the as-prepared Pd-Pt alloy hypercubic nanocrystals demonstrated an outstanding electrocatalytic activity for either methanol or formic acid electro-oxidation. In addition, accelerated CV measurement showed that the Pd-Pt nanohypercubes retained a high electrochemical stability (**Fig. S14, ESI†**).

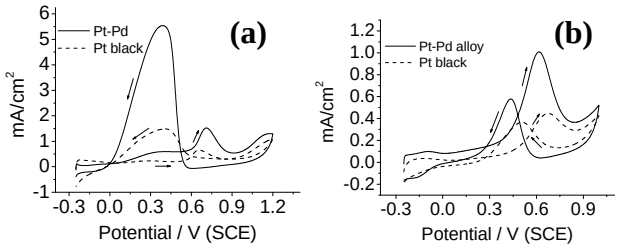

Fig. 5 CV curves for electro-oxidation of formic acid (a) and methanol (b) by the as-prepared Pd-Pt nanohypercubes and commercial Pt black. The formic acid oxidation was recorded in 0.5 M H_2SO_4 + 0.5 M HCOOH solution at a scan rate of 50mV/s between -0.25 and 1.2 V. The methanol oxidation was recorded in 0.1 M $HClO_4$ + 0.1 M CH_3OH solution at a scan rate of 50 mV/s between -0.25 and 1.0 V.

In summary, well-defined Pd-Pt alloy hypercubic nanocrystals

with an average size of 22±1.2 nm were successfully synthesized by reducing Na_2PdCl_4 and H_2PtCl_6 simultaneously in TEG with PVP as a stabilizer in the presence of an appropriate amount of KI in an one-step process under microwave irradiation for 100 sec. TEG was used as both a solvent and a reducing agent in the reaction system. It was found that the use of KI was critical to the selective synthesis of Pd-Pt alloy hypercubes. It was proposed that the preferential adsorption of I^- ions on the {100} facets and their strong coordination to Pd(II) and Pt(IV) ions were responsible for the formation of the unique Pd-Pt alloy hypercubic nanostructure by the simultaneous or sequential action of galvanic replacement and the co-deposition. Furthermore, microwave irradiation facilitated the morphology evolution by promoting the reduction, diffusion and co-deposition. Accordingly, it provided a fast and efficient route for the synthesis of alloy nanocrystals with unique morphologies. The as-prepared Pd-Pt alloy nanohypercubes improved the electrocatalytic activities.

Acknowledgements

This research was supported by the National Nature Science Foundation of China (Grant No. 21273289).

Notes and references

[a] *Key Laboratory of Catalysis and Material Science of the State Ethnic Affairs Commission & Ministry of Education, Hubei Province, College of Chemistry and Materials Science, South-Central University for Nationalities, Wuhan 430074, P. R. China. E-mail: huangt208@163.com*; *Fax: +86-27-67842752; Tel: +86-27-67843521.*

[b] *Institute of Chemistry, Chinese Academy of Science, Beijing, 100080, P. R. China.*

† Electronic Supplementary Information (ESI) available: Experimental details, TEM images, UV-vis absorbance spectra, XRD and XPS spectra. See DOI: 10.1039/b000000x/

1 *(a)* H. Zhang, M. Jin, Y. Xia, *Angew. Chem., Int. Ed*., 2012, **51**, 7656; *(b)* K. An, T. Hyeon, *Nano Today*, 2009, **4**, 359; *(c)* M. A. Mahmoud, R. Narayanan, M. A. El-sayed, *Acc. Chem. Res.*, 2013, **46**, 1795-1805; *(d)* J. W. Hong, S. W. Kang, B.-S. Choi, D. Kim, S. B. Lee, S. W. Han, *ACS Nano*, 2012, **6**, 2410; *(e)* Mahmoud, M. A. Saira, F. El-Sayed, M. A. *Nano Lett*., 2010, **10**, 3764.

2 *(a)* L. Au, Y. Chen, F. Zhou, P. H. C. Camargo, B. Lim, Z.-Y. Li, D. S. Ginger, Y. Xia, *Nano Res*., 2008, **1**, 441; *(b)* Z. Zhang, J. Hui, Z. Liu, X. Zhang, J. Zhuang, X. Wang, *Langmuir*, 2012, **28**, 14845; *(c)* X. Huang, Z. Zhao, J. Fan, Y. Tan, N. Zheng, *J. Am. Chem. Soc*., 2011, **133**, 4718; *(d)* M. Jin, H. Zhang, Z. Xie, Y. Xia, *Angew. Chem., Int. Ed.*, 2011, **50**, 7850; *(e)* T. Yu, D. Y. Kim, H. Zhang, Y. Xia, *Angew. Chem*., 2011, **123**, 2825; *(f)* J. Zhang, L. Zhang, S. Xie, Q. Kuang, X. Han, Z. Xie, L. Zheng, *Chem*., 2011, **17**, 9915; *(g)* L. Wei, Y. Fan, N. Tian, Z. Zhou, X. Zhao, B. Mao, S. Sun, *J. Phys. Chem. C*, 2012, **116**, 2040; *(h)* H. Zhang, W. Li, M. Jin, J. Zeng, T. Yu, D. Yang, Y. Xia, *Nano Lett*., 2011, **11**, 898.

3 *(a)* X. Huang, S. Tang, H. Zhang, Z. Zhou, N. Zheng, *J. Am. Chem. Soc*., 2009, **131**, 13916; *(b)* H. Zhu, Q. Chi, Y. Zhao, C. Li, H. Tang, J. Li, T. Huang, H. Liu, *Mater. Res. Bull*., 2012, **47**, 3637.

4 S. E. Skrabalak, J. Chen, Y. Sun, X. Lu, L. Au, C. Cobley, and Y. Xia, *Acc. Chem. Res*., 2008, **41**, 1587.

5 *(a)* S. Xie, N. Lu, Z. Xie, J. Wang, M. J. Kim, Y. Xia, *Angew. Chem., Int. Ed*., 2012, **51**, 10266; *(b)* B. Y. Xia, H. B. Wu, X. Wang, X. W. Lou, *Angew. Chem., Int. Ed*., 2013, **52**, 1.

6 M. Jin, H. Zhang, J. Wang, X. Zhong, N. Lu, Z. Li, Z. Xie, M. J. Kim, Y. Xia, *ACS Nano*, 2012, **6**, 2566.

7 H. Zhang, M. Jin, J. Wang, W. Li, P. H. C. Camargo, M. J. Kim, D. Yang, Z. Xie, Y. Xia, *J. Am. Chem. Soc*., 2011, **133**, 6078.

8 *(a)* X. Huang, H. Zhang, C. Guo, Z. Zhou, N. Zheng, *Angew. Chem., Int. Ed*., 2009, **48**, 4808; *(b)* J. W. Hong, S. W. Kang, B. S. Choi, D. Kim, S. B. Lee, S.W. Han, *ACS Nano*, 2012, **6**, 2410.

9 *(a)* E. Gonzalez, J. Arbiol, V. F. Puntes, *Science*, 2011, **334**, 1377; *(b)* M. A. Mahmoud, M. A. El-Sayed, *Langmuir*, 2012, **28**, 4051; *(c)* H. Zhang, M. Jin, H. Liu, J. Wang, M. J. Kim, D. Yang, Z. Xie, J. Liu, Y. Xia, *ACS Nano*, 2011, **5**, 8212.

10 G. Fu, L. Ding, Y. Chen, J. Lin, Y. Tang, T. Lu, *CrystEngComm*, 2014, **16**, 1606.

11 X. Hong, D. Wang, S. Cai, H. Rong, Y. Li, *J. Am. Chem. Soc*., 2012, **134**, 18165.

12 J. W. Hong, Y. W. Lee, M. Kim, S. W. Kang, S. W. Han, *ChemComm*, 2011, **47**, 2553.

13 C. -W. Yang, K. Chanda, P. -H. Lin, Y. -N. Wang, C. -W. Liao, and M. H. Huang, *J. Am. Chem. Soc*., 2011, **133**, 19993.

14 *(a)* X. M. Lu, L. Au, J. McLellan, Z. Y. Li, M. Marquez, Y. N. Xia, *Nano Lett*., 2007, **7**, 1764 ; *(b)* M. McEachran, D. Keogh, B. Pietrobon, N. Cathcart, I. Gourevich, N. Coombs, V. Kitaev, *J. Am. Chem. Soc*., 2011, **133**, 8066; *(c)* H. J. Fan, U. Gçsele, M. Zacharias, *Small*, 2007, **3**, 1660; *(d)* W. Wang, M. Dahl, Y. Yin, *Chem. Mater*., 2013, **25**, 1179.

15 *(a)* W. Tu, H. Liu, *J. Mater. Chem*., 2000, **10**, 2207 ; *(b)* M. Tsuji, M. Hashimoto, Y. Nishizawa, M. Kubokawa, T. Tsuji, *Chem. Eur. J*., 2005, **11**, 440; *(c)* Y. Yu, Y. Zhao, T. Huang, H. Liu, *Pure Appl. Chem*., 2009, **81**, 2377; *(d)* Y. Yu, Y. Zhao, T. Huang, H. Liu, *Mater. Res. Bull*., 2010, **45**, 159; *(e)* L. Dai, Q. Chi, Y. Zhao, H. Liu, Z. Zhou, J. Li, T. Huang, *Mater. Res. Bull*., 2014, **49**, 413.

16 Y. Xia, E. Kim, G. M. Whitesides, *J. Electrochem. Soc*., 1996, **143**, 1070.

17 J. Langford, A. Wilson, *J. Appl. Cryst*., 1978, **11**, 102.

18 C. D. Wagner, W. M. Riggs, L. E. Davis, J. F. Moulder, B. E. Muilenberg. *Handbook of X-ray Photoelectron Spectroscopy*, Perkin-Elmer, Physical Electronics Division, Eden Prairie, 1979.

19 B. L. Hayes, *Aldrichimica ACTA*, 2004, **37**, 66-77.

20 a) Y. J. Xiong, H. G. Cai, B. J. Wiley, J. G. Wang, M. J. Kim, Y. N. Xia, *J. Am. Chem. Soc*., 2007, **129**, 3665; b) X. Huang, N. Zheng, *J. Am. Chem. Soc*., 2009, **131**, 4602; c) X. Huang, S. Tang, X. Mu, Y. Dai, G. Chen, Z. Zhou, F. Ruan, Z. Yang and N. Zheng, *Nature Nanotech*., 2011, **6**, 28; d) M. Chen, B. H. Wu, J. Yang, N. F. Zheng, *Adv. Mater*., 2012, **24**, 862; e) S. E. Lohse, N. D. Burrows, L. S.carabelli, L. M. Liz-Marzan, C. J. Murphy, *Chem. Mater*., 2014, **26**, 34 ; f) J. S. DuChene, W. Niu, J. M. Abendroth, Q. Sun, W. Zhao, F. Huo, and W. D. Wei, *Chem. Mater*., 2013, **25**, 1392; g) A. Carrasquillo, J. J. Jeng, R. J. Barriga, W. F. Temesghen, M. P. Soriaga, Inorg. Chim. Acta 1997, 255, 249.

21 *(a)* J. Solla-Gullón, F. J. Vidal-Iglesias, E. Herrero, J. M. Feliu, A. Aldaz, *Electrochem. Commun.*, 2006, **8**, 189; *(b)* M. Hara, U. Linke, T. Wandlowski, *Electrochim. Acta.*, 2007, **52**, 5733.